Scalable risk assessment of large infrastructure systems with spatially correlated components

Diqi Zeng[a,1], Hao Zhang[*,a,2], Hongzhe Dai[b,3], Michael Beer[c,4]

[a]*School of Civil Engineering, The University of Sydney, NSW 2006, Australia*
[b]*School of Civil Engineering, Harbin Institute of Technology, Harbin 150090, China*
[c]*Institute for Risk and Reliability, Leibniz Univ. Hannover, 30167 Hannover, Germany; Institute for Risk and Uncertainty, Univ. of Liverpool, Liverpool L69 3BX, United Kingdom; International Joint Research Center for Engineering Reliability and Stochastic Mechanics, Tongji Univ., Shanghai 200092, China*

Abstract

Risk assessment of spatially distributed infrastructure systems under natural hazards shall treat the performance of individual components as stochastically correlated due to the common engineering practice in the community including similarities in building design code, regulatory practices, construction materials, construction technologies, and the practices of local contractors. Modelling the spatially correlated damages of an infrastructure system with many components can be computationally expensive. This study addresses the scalability issue of risk analysis of large-scale systems by developing an interpolation technique. The basic idea is to sample a portion of components in the systems and evaluate their correlated damages accurately, while the damages of remaining components are interpolated from the sampled

[*]Corresponding author
[1]E-mail address: dzen5770@uni.sydney.edu.au
[2]E-mail address: hao.zhang@sydney.edu.au
[3]E-mail address: hzdai@hit.edu.cn
[4]E-mail address: beer@irz.uni-hannover.de

components. The new method can handle not only linear systems, but also systems with complex connectivity such as utility networks. Two examples are presented to demonstrate the proposed method, including cyclone loss assessment of the building portfolios in a virtual community, and connectivity analysis of an electric power system under a scenario cyclone event.

Key words: Probabilistic risk assessment, Community resilience, Random field, Structural reliability

---

1. Introduction

Civil infrastructure systems such as building portfolios, transportation systems and utility networks provide essential support to the well-being of a community, and are susceptible to natural hazards such as tropical cyclones and earthquakes. The damages and failures of infrastructure systems lead to not only direct economic loss resulting from repair and reconstruction, but also indirect economic loss such as population dislocation and employment loss. To advocate a whole-of-community approach of hazard mitigation, community resilience assessment has become internationally an imperative [1]. The resilience of a community is defined by the ability of its physical and non-physical infrastructure, which includes built environment, social institutions, and its people, to return to a level of normalcy within a reasonable time following the occurrence of an event [1]. A fundamental task for community resilience assessment is to conduct damage assessment of distributed infrastructure systems under a large-scale natural hazard. The results of damage assessment provide the initial conditions of a community right after a hazard, which can be used to further assess the social and economic impact of the hazard during post-hazard recovery period. Infrastructure system losses are uncertain in nature due to the stochastic variability in hazard demands and system capacities. The uncertainties must be thoroughly understood to facilitate risk-informed decision making.

The state of the art in risk assessment of individual infrastructure facilities is reasonably mature. The capacities of infrastructure facilities against a specific hazard demand are modelled by their fragility functions. The fragility function of a structure provides its conditional probability of reaching a particular damage state given a specific hazard demand. In previous studies, fragility functions were typically developed independently for different structural types such as Lee and Rosowsky [2] and Li and Ellingwood [3]. However, in risk assessment of distributed infrastructure systems, the fragility functions of individual components should be modelled as stochastically correlated. The spatial correlation arises due to the similarities of individual components in construction materials, regulatory practices, structural design, construction technologies, and construction practices of local contractors over a community [4].

Significant progress has been made in risk assessment of distributed infrastructure systems considering the spatial correlation of damages to individual components. The spatial correlation of infrastructure components may arise due to the spatial correlation of hazard demands placed by a natural hazard with a large geographic footprint and the spatial correlation of structural fragilities in a community. Most previous studies focused on the impact of the spatial correlation of hazard demands placed by an earthquake event in system risk assessment, such as building portfolio risk [5–8] and lifeline system risk [9–11]. An initial effort has also been made to consider the spatial correlation of wind speeds from a tropical cyclone event in system risk assessment [12]. Compared with studies on the spatial correlation of hazard demands, the studies on the spatial correlation of structural fragilities are relatively limited [4, 13–16]. Lee and Kiremidjian [13] examined the effect of the fragility correlation between bridges on the total repair cost of a bridge network subjected to a scenario earthquake. A simple equi-correlation assumption was applied to the fragility correlation and the sensitivity of the repair cost to the correlation was investigated. Wang et al. [16] also adopted an equi-correlation assumption for the fragility correlation between buildings in evaluating cyclone damage cost to a community's residual buildings. Vitoontus and Ellingwood [4] were among the first to mathematically model the fragility correlation between buildings in an urban area as a function of material, structural type, building code, and workmanship in construction. The correlation of fragilities was included in the evaluation of repair cost to building portfolios under a scenario earthquake. In general, the impact of the correlation between individual structures in system risk assessment depends on the system loss metric selected. Many previous studies evaluated the linear loss metrices of infrastructure systems, such as the summed economic losses of individual buildings [4–6, 16]. In this case, ignoring the correlation does not change the mean loss, but would underestimate the uncertainty of the loss. However, for nonlinear loss metrices such as the power outage ratio of an electric power grid (a connectivity problem), ignoring the correlation would affect both the mean and variance of the loss estimate. This point was also observed in other studies [12, 17]

Previous system risk studies typically modelled an infrastructure system in an individual component basis, e.g., bridge networks [13, 18] and building portfolios [5, 19]. Considering the performance of each component as correlated, the analysis needs to handle a correlation matrix of size of $N \times N$, which N denoted the number of the components in the systems. Modelling the correlated components can become computationally infeasible if the system has a large number of components. To overcome the computational cost issue, a random sampling technique has been proposed [4] for evaluating the repair cost of building portfolios. In this technique, a small number of buildings are randomly sampled. The loss of the sampled buildings is computed and scaled by the ratio between the total building number and the sampled building number to approximate the total loss of the building portfolio. The random sampling technique was also used by Lin and Wang [20] to evaluate the resilience of building portfolios. The accuracy of the random sampling technique deteriorates if the building portfolio becomes more heterogeneous. Most importantly, the random sampling technique cannot capture the connectivity of lifeline networks. For example, in functional loss assessment of an electric power system, individual components, such as distribution substations and transmission line support structures, are interconnected in such a way that a structurally undamaged facility may lose its function due to the failures of other facilities. To capture the failures of undamaged facilities, the damage states of all the interconnected components are required. Since the random sampling technique only captures damages of sampled components, it cannot be used to evaluate the risk of lifeline networks. New approaches are needed to address the scalability issue of risk assessment.

In this paper, an interpolation technique is developed to evaluate the correlated damages of a large-scale infrastructure system. The basic idea is to sample a portion of components in the system and evaluate their correlated damages accurately, while the damages of remaining components are interpolated from the sampled components. The idea of interpolation originates from random field discretization techniques in stochastic finite element methods. The optimal linear estimation (OLE) method, originally developed for continuous random fields [21], is improved to simulate the random vector of component damages. Due to the interpolation, the size of the correlation matrix required to analyze the system is reduced remarkably, making the proposed method suitable to systems of large size. Two examples are provided to demonstrate the proposed method, including cyclone loss assessments of building portfolios in a virtual community, and an electric power system with interconnected infrastructure components. In the first example, cyclone-induced damages to individual buildings are considered. Focused samples are selected uniformly at random from each building type in each building zone. In Example 2 (power grid), damages to transmission support structures are considered. Focused transmission structures include all the structures located at the intersections of the transmission lines, and the remaining focused structures are randomly sampled along each transmission line.

2. Monte Carlo simulation of spatially correlated damages

Let D denote the damage state of a structure. D is a discrete random variable and typically taken as different numerical values for different damage states, e.g., $D = 0$ for no damage, $D = 1$ for minor damage, and $D = 2$ for moderate damage. In a large infrastructure system such as a building portfolio or utility network, the damage states of individual components are invariably positively correlated due to common engineering practices [4]. In order to compute the probabilistic characteristics of the collective loss/damage of an infrastructure system, the joint probabilities of individual components' damage states are required. However, only knowing the fragility functions of the components and their correlations is insufficient to determine the joint probabilities. In general, using copulas to approximate the stochastic dependence of structural damages is required. To the best of our knowledge, all previous studies [4, 14–16] regarding modelling spatially correlated damages of multiple structures explicitly or implicitly adopted Gaussian copulas to model the stochastic dependence of the structures, where correlated damage states are converted into correlated Gaussian random variables. Currently, there is no data available to justify if the stochastic dependence of structural damages is Gaussian or not. Using Gaussian copulas is mainly due to its computational feasibility. Using non-Gaussian copulas to capture the correlation of random variables is computationally feasible only if the number of the variables is relatively small, e.g., 2 correlated random variables [22]. A recent work [23] developed a method to construct the joint probability density function (PDF) of multiple random variables using non-Gaussian copulas, when marginal distributions and correlations are specified. In this method, a joint PDF is expressed in terms of pairwise bivariate copula density functions and the pair copulas are determined based on a particular vine structure. The method was demonstrated by the examples of system reliability analysis with up to 8 random variables. However, risk assessment of infrastructure systems typically involves a large number of correlated random variables and constructing the joint PDF of these variables by non-Gaussian copulas is still computationally difficult.

In this study, a Gaussian copula is used to model the stochastic dependence among the components [4, 15]. Let q_{ij} denote the correlation coefficient between the damages of components i and j. Consider an infrastructure system with N components. Let U_i denote the hazard intensity for component i. For a set of given hazard intensities $(U_1, \ldots, U_N)$, the procedures to generate the correlated damage states $(D_1, \ldots, D_N)$ by Monte Carlo simulation (MCS) and copula are as follows [4, 15],

Step 1: Generate N correlated standard Gaussian random variables, $s_1, \ldots, s_N$, with a correlation coefficient matrix $\boldsymbol{W} = [q_{ij}]$.

Step 2: Transform $s_1, \ldots, s_N$ into the samples of standard uniformly distributed random variables $x_1, \ldots, x_N$, by $x_i = \Phi(s_i)$, in which $\Phi(\cdot)$ represents the cumulative distribution function of a standard normal.

Step 3: Map the samples of damage states $D_1, \ldots, D_N$ from $x_1, \ldots, x_N$ by $D_i = v$, if $P(D_i \leq v - 1|U_i = u_i) < x_i \leq P(D_i \leq v|U_i = u_i)$.

In Step 3, $P(\cdot)$ represents the probability of the event in the bracket; $D_i = v-1$ represents the damage state that is one-level less severe than the damage state of v; if v is already the lowest damage state, $P(D_i \leq v - 1|U_i = u_i) = 0$. To specify q_{ij} in Step 1, the exponential form of fragility correlation model is taken from the literature [4]. More discussion about the correlation model will be given in the next section. It should be noted that this paper will develop a general method to simulate the correlated damages of a large-scale distributed infrastructure system. The correlation model itself is not the focus. In simulating the correlated damages of all components, the main computational cost comes from Step 1. The correlation coefficient matrix $\boldsymbol{W}$ has a size of $N \times N$ and it would become computationally costly for large-scale systems.

3. A new interpolation-based method for simulating correlated damages

3.1. Optimal linear estimation method for random field discretization

As discussed in Section 2, a key step to simulate the correlated damage of a large-scale infrastructure system is to simulate a high-dimension vector of correlated standard Gaussian random variables. One idea to reduce the computational cost is to apply interpolation techniques of random field discretization. In this method, only some components are sampled, and based on which the remaining components are interpolated. Random field discretization with interpolation techniques has been used in stochastic finite element methods to represent continuous random fields such as structural material properties with spatial variability.

One of the interpolation technique for random field discretization is the Optimal linear estimation (OLE) method [21]. We start with the original OLE method for generating N correlated standard Gaussian random variables. Among the N components, assume that M components have been generated and denoted as $\boldsymbol{s}_o = \{S_k\}$, $k = 1, \ldots, M$. The remaining $N - M$ components are represented by $\boldsymbol{s}_* = \{S_i\}$ where $i = M+1, ..., N$. S_i can be interpolated from $\boldsymbol{s}_o$ using OLE as follows [21],

$$S_i^{'} = \overline{S}_i + \boldsymbol{d}_i^{\mathrm{T}} \boldsymbol{G}^{-1} (\boldsymbol{s}_o - \boldsymbol{\mu}), \tag{1}$$

in which $S_i^{'}$ is the interpolated value of S_i; $\overline{S}_i$ represents the mean of S_i; $\boldsymbol{d}_i$ is an M-dimension vector containing the covariance between S_i and the elements of $\boldsymbol{s}_o$; $\boldsymbol{G}$ is the covariance matrix of $\boldsymbol{s}_o$; $\boldsymbol{\mu}$ is an M-dimension vector containing the mean values of $\boldsymbol{s}_o$, i.e., $\boldsymbol{\mu} = \{\overline{S}_1, \ldots, \overline{S}_M\}$. If $\boldsymbol{G}$ is empirically formed to represent the correlation of real infrastructure items, it may not satisfy the requirements of covariance matrices, which is not permissible in simulating correlated random variables. Thus, empirically estimated correlation coefficients are typically fitted to a mathematically feasible correlation model, such as the exponential model later discussed in this study. Alternatively, an empirically formed correlation matrix can be adjusted to a mathematically feasible correlation matrix using the algorithm of Higham [24]. Then $\boldsymbol{G}$ is inversible. Eq. (1) requires the inverse of matrix $\boldsymbol{G}$. It is noted that for the generation of $\boldsymbol{s}_o$, the spectral decomposition of $\boldsymbol{G}$ would be determined [25]. Given the spectral decomposition, $\boldsymbol{G}^{-1}$ can be obtained by simply inverting the diagonal matrix which includes the eigen-values of $\boldsymbol{G}$.

Since $S_i^{'}$ is a linear transformation of Gaussian random vector $\boldsymbol{s}_o$, $S_i^{'}$ is also a Gaussian random variable. The mean of $S_i^{'}$ is given as

$$\begin{aligned} \mathrm{E}(S_i^{'}) &= \mathrm{E}\left(\overline{S}_i + \boldsymbol{d}_i^{\mathrm{T}} \boldsymbol{G}^{-1} (\boldsymbol{s}_o - \boldsymbol{\mu})\right) \\ &= \overline{S}_i + \boldsymbol{d}_i^{\mathrm{T}} \boldsymbol{G}^{-1} \mathrm{E}\left(\boldsymbol{s}_o - \boldsymbol{\mu}\right) \\ &= \overline{S}_i, \end{aligned} \tag{2}$$

in which $\mathrm{E}(\cdot)$ represents the expectation. Eq. (2) shows that $S_i^{'}$ and S_i have the same mean value, indicating that OLE is unbiased.

The covariance between two interpolated variables $S_i^{'}$ and $S_j^{'}$ $(i, j = M + 1, ..., N)$, denoted as δ_{ij}, is given by

$$\delta_{ij} = \boldsymbol{d}_i^{\mathrm{T}} \boldsymbol{G}^{-1} \boldsymbol{d}_j. \tag{3}$$

The variance of $S_i^{'}$, denoted by $\sigma_i^{'2}$, is obtained from Eq. (3) by taking $i = j$. The correlation between $S_i^{'}$ and $S_j^{'}$, denoted as ρ_{ij}, is given as

$$\rho_{ij} = \frac{\delta_{ij}}{\sigma_i^{'} \sigma_j^{'}}. \tag{4}$$

The variance of $\epsilon_i = S_i - S_i^{'}$, denoted as $\sigma_{\epsilon_i}^2$, is as follows,

$$\begin{aligned}
\sigma_{\epsilon_i}^2 &= \mathrm{E}\left[(S_i - S_i^{'})^2\right] \\
&= \mathrm{E}\left\{\left[S_i - \mu_i - \boldsymbol{d}_i^{\mathrm{T}} \boldsymbol{G}^{-1} (\boldsymbol{s}_o - \boldsymbol{\mu})\right]^2\right\} \\
&= \sigma_i^2 - \boldsymbol{d}_i^{\mathrm{T}} \boldsymbol{G}^{-1} \boldsymbol{d}_i \\
&= \sigma_i^2 - \sigma_i^{'2}
\end{aligned} \tag{5}$$

where σ_i^2 and $\sigma_i^{'2}$ are the variance of S_i and $S_i^{'}$, respectively. It can be seen that $\sigma_i^{'2}$ is always smaller than σ_i^2.

The OLE method was initially developed to simulate continuous Gaussian random fields. Li and Der Kiureghian [21] suggested that the accuracy of OLE deteriorates for a nondifferentiable random field whose correlation function $q\left(\boldsymbol{x}, \boldsymbol{x}^{'}\right)$ for sites $\boldsymbol{x}$ and $\boldsymbol{x}^{'}$ does not have a zero slope at $\boldsymbol{x} = \boldsymbol{x}^{'}$. The damage of individual components of a large system is a random vector, and may not be differentiable. For example, a common function to represent the correlations of structural fragility is taken from the literature [4, 15, 20] as follows,

$$q\left(\boldsymbol{x},\boldsymbol{x}^{'}\right)=\begin{cases} a\cdot\exp\left(-\frac{|\boldsymbol{x}-\boldsymbol{x}^{'}|}{b}\right)+r & \text{if} \quad \boldsymbol{x}\neq\boldsymbol{x}^{'}, \\ 1 & \text{if} \quad \boldsymbol{x}=\boldsymbol{x}^{'}, \end{cases} \tag{6}$$

where a, b and r are model parameters. In the study of Vitoontus and Ellingwood [4], the correlation length b is a constant, a and r depend on two buildings' similarities in construction material, structural type, storey range and design code. Random fields with a correlation function of Eq. (6) are generally non-differentiable.

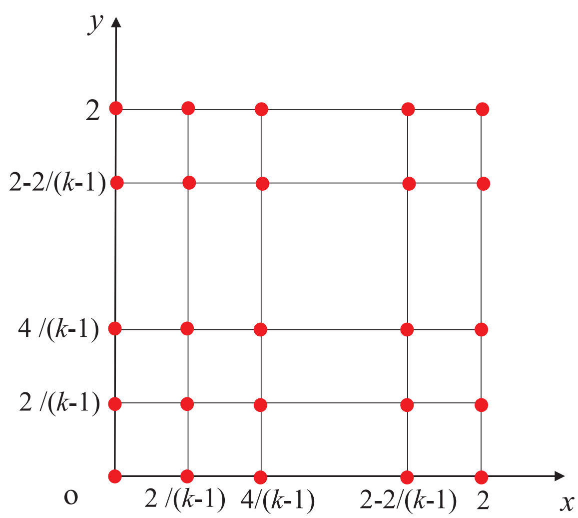

Figure 1: The distribution of sampled points in the random field.

To investigate OLE's accuracy for non-differentiable random fields, consider a standard Gaussian random field $S(\boldsymbol{x})$ with a correlation function of Eq. (6), in which the parameters a, r ,b are taken as 0.7, 0 and 1. The random field is defined in a Cartesian coordinate system (x, y) with $0 \leq x \leq 2$

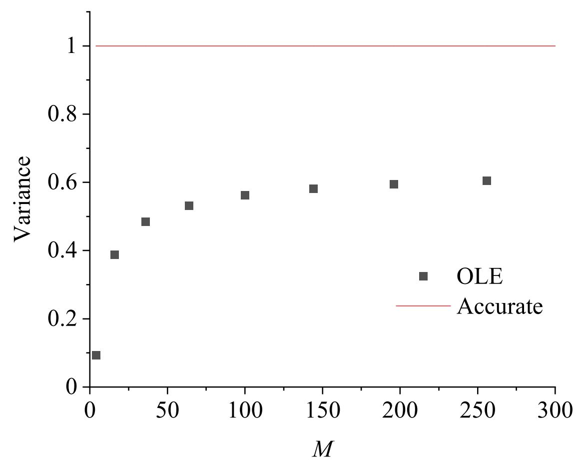

Figure 2: The variance of point A=(1,1) from OLE, interpolated from M sample points.

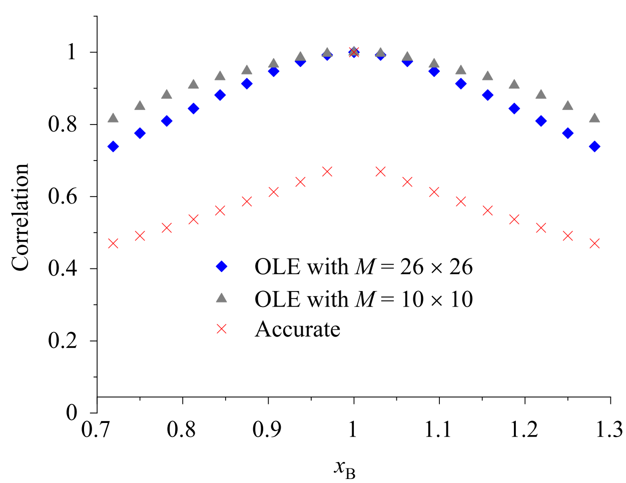

Figure 3: The accuracy of OLE in solving correlation between interpolated points $\mathrm{A} = (1, 1)$ and $\mathrm{B} = (x_\mathrm{B}, x_\mathrm{B})$.

and $0 \leq y \leq 2$. A total of M points are selected and they are arranged such that in each orthogonal direction there are k equally spaced points ($M = k \times k$), as shown in Fig. 1. Consider point A, located in (1,1). Point

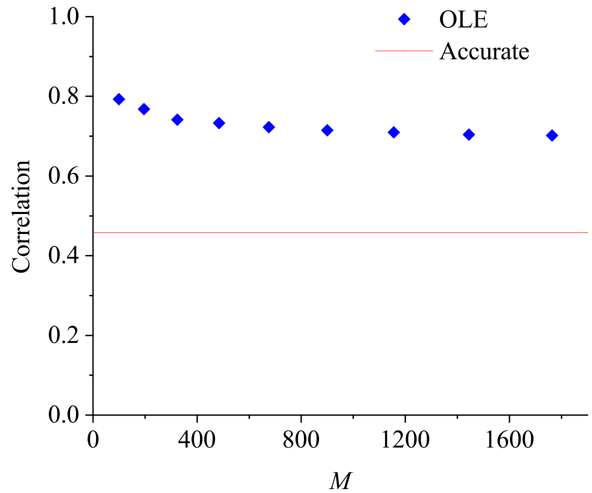

Figure 4: The accuracy of OLE in solving the correlation of A $= (1, 1)$ and C $= (0.7, 0.7)$, given different number of sampled points.

A is interpolated using the M sampled points. The variances of point A from OLE with different M are plotted in Fig. 2. It can be seen that the variance of OLE is always smaller than the true variance and does not converge with increasing M. Next, consider another interpolation point B, with a coordinate of $(x_{\mathrm{B}}, x_{\mathrm{B}})$. The correlation coefficient of points A and B is plotted in Fig. 3 for two cases, i.e., $M = 10 \times 10$ and $M = 26 \times 26$. In both cases, significant error is observed. Also, the correlation coefficients of point A and point C $= (0.7, 0.7)$ given different M are plotted in Fig. 4. The correlation of OLE is always higher than the true correlation and does not converge with increasing M. These results demonstrate that in simulating a non-differentiable Gaussian random field, the original OLE underestimates the variance of an interpolation point, and overestimates the correlation of two interpolation points.

3.2. Improved OLE technique

This study proposes an improved OLE technique, referred to as IOLE, suitable for non-differentiable Gaussian random fields. In the IOLE, the interpolated value of S_i, denoted by $\tilde{S}_i$, is given by

$$\tilde{S}_i = S_i^{'} + \zeta_i \cdot (\sigma_i^2 - \sigma_i^{'2})^{0.5}, \tag{7}$$

in which $S_i^{'}$ and $\sigma_i^{'2}$ are obtained from the original OLE, i.e., Eq. (1) and Eq. (3) respectively; σ_i^2 is the accurate variance at point i; and ζ_i is an independent standard Gaussian random variable. Since the mean of the second term in Eq. (7) is zero, the mean of $\tilde{S}_i$ is equal to the mean of $S_i^{'}$, thus $\tilde{S}_i$ is also unbiased. The covariance of two interpolated points $\tilde{S}_i$ and $\tilde{S}_j$, denoted as $\tilde{\delta}_{ij}$, is equal to

$$\begin{aligned} \tilde{\delta}_{ij} =& \mathrm{E}\left(\left(\tilde{S}_i - \mathrm{E}(\tilde{S}_i)\right)\left(\tilde{S}_j - \mathrm{E}(\tilde{S}_j)\right)\right) \\ =& \mathrm{E}(S_i^{'}S_j^{'}) - \mathrm{E}(S_i^{'})\mathrm{E}(S_j^{'}) + \mathrm{E}(\zeta_i\zeta_j)\sqrt{(\sigma_i^2 - \sigma_i^{'2})(\sigma_j^2 - \sigma_j^{'2})}, \end{aligned} \tag{8}$$

and

$$\tilde{\delta}_{ij} = \begin{cases} \boldsymbol{d}_i^{\mathrm{T}}\boldsymbol{G}^{-1}\boldsymbol{d}_j & \text{if} \quad i \neq j \\ \sigma_i^2 & \text{if} \quad i = j. \end{cases} \tag{9}$$

Eqs. (8) and (9) show that if $i \neq j$, $\tilde{\delta}_{ij}$ is the same as the covariance obtained by the original OLE. If $i = j$, $\tilde{\delta}_{ij}$ represents the variance of $\tilde{S}_i$ and is equal to the accurate variance of point i (σ_i^2).

To demonstrate the accuracy of IOLE, the example of standard Gaussian random field presented in the last section is repeated using the IOLE. The variances of interpolated point A $= (1, 1)$ using OLE and IOLE, as well as the

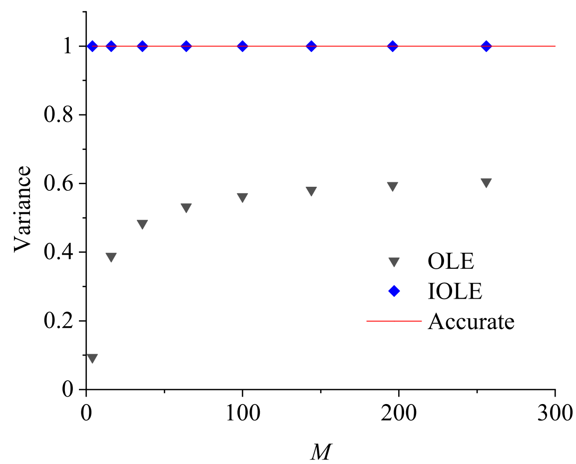

Figure 5: Comparison of IOLE and OLE: variance of point A=(1,1) interpolated from M sample points.

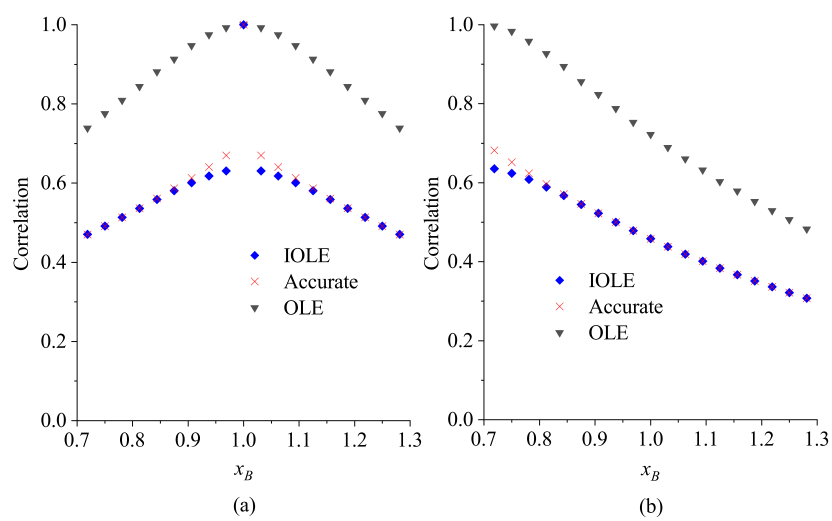

Figure 6: Comparison of IOLE and OLE: correlation coefficient of (a) points A=(1,1) and $\mathrm{B} = (x_\mathrm{B}, x_\mathrm{B})$ and (b)points C=(0.7,0.7) and $\mathrm{B} = (x_\mathrm{B}, x_\mathrm{B})$.

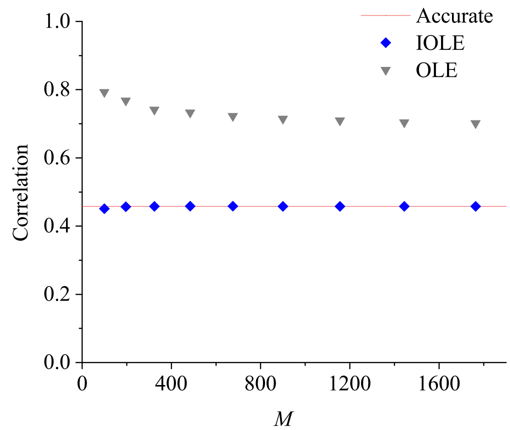

Figure 7: Comparison of IOLE and OLE in solving correlation given different number of sampled points.

true variance, are given in Fig. 5. It can be seen that compared to the original OLE, the IOLE represents a significant improvement in approximating the variance of an interpolated point. Fig. 6 gives the correlation coefficient of two interpolation points $\mathrm{A} = (1, 1)$ and $\mathrm{B} = (x_{\mathrm{B}}, x_{\mathrm{B}})$ by using $M = 26 \times 26$ sampled points and that of two interpolation points $\mathrm{C} = (0.7, 0.7)$ and $\mathrm{B} = (x_{\mathrm{B}}, x_{\mathrm{B}})$. The correlation obtained by IOLE is considerably more accurate than that obtained by OLE. For example, the accurate correlation of A=(1,1) and B=(0.91,0.91) is 0.61. The correlation obtained by IOLE is 0.60, while the correlation obtained by OLE is 0.95. The correlation between $\mathrm{C} = (0.7, 0.7)$ and $\mathrm{A} = (1, 1)$ by using various numbers of sampled points, are given in Fig. 7. The correlation obtained by IOLE becomes essentially the same as the accurate correlation if M reaches 200. However, the correlation obtained by OLE does not converge to the accurate correlation.

4. Example 1: damage assessment of building portfolios in Centerville under a scenario cyclone

The first example is to evaluate the cyclone damage of the building portfolios in the Centerville Virtual Community Testbed [26]. A scenario-based risk assessment approach is adopted, in which a single postulated cyclone event is used as hazard input. The cyclone damage is measured by the cost ratio, Z, of the building portfolios. Z is defined as the ratio of total repair costs to the total replacement costs,

$$Z = \frac{\sum_{l=1}^{L}\sum_{i=1}^{n_l} R_{il} w_{il}}{\sum_{l=1}^{L}\sum_{i=1}^{n_l} w_{il}}, \tag{10}$$

in which L represents the number of occupancy classes; n_l represents the number of buildings of occupancy class l; w_{il} is the replacement cost of building i of occupancy class l; R_{il} is the cost ratio of building i of occupancy class l and is a function of the building's damage state. In this study, the replacement cost w_{il} of individual building is considered as deterministic, while the cost ratio R_{il} is treated as a random variable. The building portfolio cost ratio Z is the weighted average of the cost ratios to individual buildings. The weighting coefficients are deterministic, while the cost ratios are random. Thus, the expectation of Z is equal to the weighted average of the expected cost ratios to individual buildings, as follows

$$\mathrm{E}(Z) = \frac{\sum_{l=1}^{L}\sum_{i=1}^{n_l} \mathrm{E}(R_{il}) w_{il}}{\sum_{l=1}^{L}\sum_{i=1}^{n_l} w_{il}}. \tag{11}$$

Eq. (11) shows that $\mathrm{E}(Z)$ is independent of the spatial correlation among individual buildings. However, the standard deviation of Z would depend on the spatial correlation of individual buildings. The standard deviation of Z,

σ_Z, is given by

$$\sigma_Z = \frac{(\sum_{l=1}^{L}\sum_{i=1}^{n_l}\sigma_{il}^2 w_{il}^2 + \sum_{i_1\neq i_2 \text{or} l_1\neq l_2}\rho_{i_1l_1,i_2l_2}\sigma_{i_1l_1}\sigma_{i_2l_2}w_{i_1l_1}w_{i_2l_2})^{0.5}}{\sum_{l=1}^{L}\sum_{i=1}^{n_l}w_{il}}, \quad (12)$$

where σ_{il} is the standard deviation of the cost ratio R_{il} to building i in occupancy class l; $\rho_{i_1l_1,i_2l_2}$ is the correlation coefficient of $R_{i_1l_1}$ and $R_{i_2l_2}$.

4.1. Description of Centerville

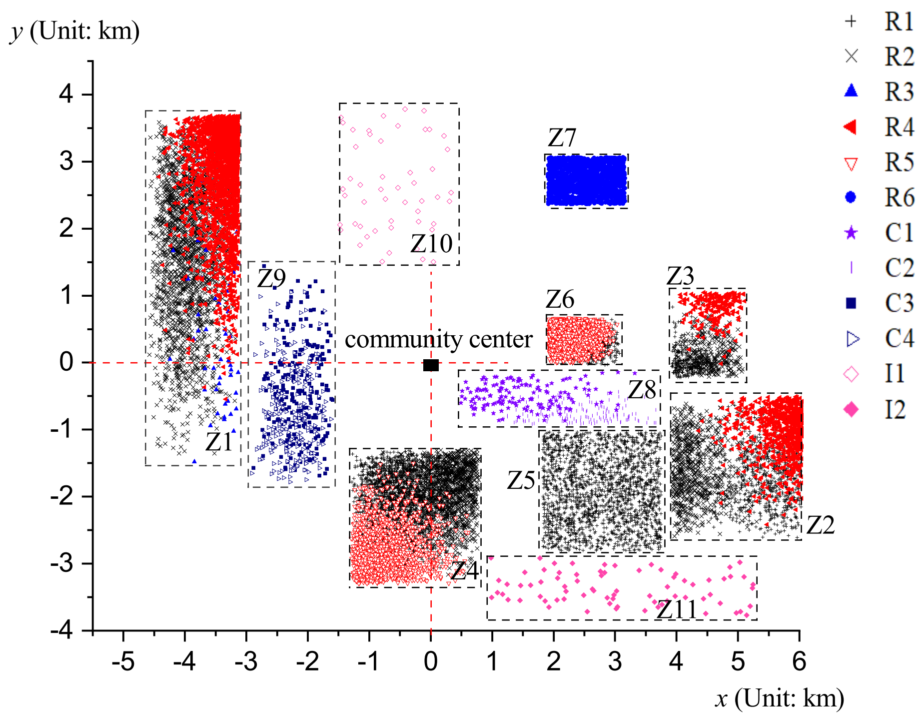

Figure 8: Example 1: building inventory of Centerville.

Centerville represents a typical middle-class city in the USA [26]. It has a size of roughly 13×8 km^2. The building inventory includes 12 basic building types, distributed in 11 zones, as shown in Fig. 8. Z1-Z7 are residential zones, while Z8 and Z9 are business zones and Z10 and Z11 are industrial zones.

Table 1: Example 1: descriptions of building types [26, 27].

Occupancy	ID	Description
Residential	R1	1-storey, Unreinforced masonry, Single-family, 1400 ft^2, 1945-1970
	R2	1-storey, Unreinforced masonry, Single-family, 2400 ft^2, 1985-2000
	R3	2-storey, Wood frame, Single-family, 3200 ft^2, 1985-2000
	R4	1-storey, Unreinforced masonry, Single-family, 2400 ft^2, 1970-1985
	R5	3-storey, Wood frame, Multi-family, 12,000 ft^2/floor, 1985
	R6	Single-family, Mobile home
Commercial	C1	1-storey, Steel, 50,000 ft^2, 1980
	C2	2-storey, Steel, 50,000 ft^2, 1980
	C3	2-storey, Steel, 25,000 ft^2, 1960
	C4	Steel, 125,000 ft^2, 1995
Industrial	I1	2-storey, Reinforced masonry, 100,000 ft^2, 1975
	I2	1-storey, Reinforced masonry, 500,000 ft^2, 1995

ft^2= 0.0929 m^2

The building information is adopted from Ellingwood et al. [26]. Table. 1 summarizes the descriptions of 12 types of buildings considered in Ellingwood et al. [26]. In total, 20,609 buildings are distributed in 11 zones. The number of buildings of each type in each building zone is summarized in Table 2. In a given zone, buildings are located randomly; It is assumed that buildings of the same type are more likely adjacent to each other, and their locations have a correlation coefficient of 0.6. Fig. 8 shows the assumed distribution of the 20,609 buildings, generated by a MCS run.

Table 2: The number of buildings of each type in each building zone [26].

ID	Z1	Z2	Z3	Z4	Z5	Z6	Z7	Z8	Z9	Z10	Z11
R1	0	767	300	2567	1856	700	0				
R2	2000	700	300	1000	0	0	0				
R3	50	0	0	0	0	0	0				
R4	2196	800	200	0	0	0	0				
R5	0	0	0	1200	0	3696	0				
R6	0	0	0	0	0	0	1352				
C1								150	0		
C2								150	0		
C3								0	250		
C4								0	250		
I1										50	0
I2										0	75

The wind fragility functions of the 12 building types have been studied by Wang [27], based on HAZUS-MH [28]. The fragility functions consider the damages of roof cover, roof sheathing panels, windows, doors, and wall sections. Four damage states are considered, with $D = 0$, 1, 2, and 3 representing insignificant, moderate, severe and complete damage states, respectively.

The fragility functions have a form of lognormal function as follows,

$$P(D \geq v|U = u) = \Phi\left(\frac{\ln(u) - \lambda_v}{\xi_v}\right), \tag{13}$$

in which U represents the wind speed; the two parameters λ_v and ξ_v of each building type are taken from Wang [27] and summarized in Table 3.

The replacement costs w for a given type of building are assumed deterministic [27], and the values are summarized in Table 3. The functional relation between the damage state D and cost ratio R is taken from Wang [27], i.e., $R = 0$ for $D = 0$, $R = 0.2$ for $D = 1$, $R = 0.4$ for $D = 2$, and $R = 0.8$ for $D = 3$. In general, the (functionality/economic) loss is a function of structural damage state and the damage value conditioned on the damage state. In reality, uncertainties exist in the loss for a given damage state, thus the conditional damage value shall also be modelled as a random variable. The present study only considers the uncertainty in damage states, while treats the conditional damage value as deterministic. It is because: 1) there is a lack of data to estimate the damage value uncertainty, and 2) in some previous studies, uncertainty in conditional damage value was ignored (e.g., Goda and Hong [5]; Vitoontus and Ellingwood [4]). The present study follows the same assumption.

The fragility correlation q_{ij} for buildings i and j ($i \neq j$) is modelled as [4]

$$q_{ij} = a \cdot \exp(-\frac{h_{ij}}{b}) + r \tag{14}$$

where h_{ij} is the separation distance between buildings i and j; a, r and b are model parameters, with b also known as correlation length. The parameters a and r are considered dependent of the similarity between two buildings in material and design code, and the correlation length b is considered as

Table 3: Example 1: wind fragility functions (wind speed unit: m/s) and replacement costs w [27].

ID	w ($US)	λ_1	λ_2	λ_3	ξ_v $(v = 1, 2, 3)$
R1	80,430	3.8906	4.0217	4.1375	0.1097
R2	137,880	4.1137	4.2448	4.3606	0.1097
R3	183,840	3.9510	4.0732	4.1661	0.0998
R4	137,880	4.0084	4.1394	4.2552	0.1097
R5	2,068,200	3.9582	4.1405	4.1814	0.0998
R6	63,000	4.2460	4.3770	4.4200	0.1295
C1	2,872,500	3.9776	4.0729	4.6035	0.0799
C2	2,872,500	3.8822	3.9775	4.5082	0.0799
C3	1,436,250	3.7769	3.8722	4.4028	0.0799
C4	7,181,250	3.8822	3.9775	4.5082	0.0799
I1	5,745,000	3.6624	3.7486	3.9014	0.1393
I2	28,725,000	3.8765	3.9627	4.1156	0.1393

constant for the whole community [4]. For demonstration purpose, the correlation length b is taken as 2 km, roughly equal the average dimention of each building zone. The values of a, b and r used in this example are summarized in Table. 4. It is assumed that R2 and R3, C1 and C2 were designed using the same generations of building codes. Sensitivity analysis on correlation length b will be conducted in the next section.

Table 4: Example 1: model parameters of fragility correlation.

Building description	a	r	b (Unit: km)
Same materials; Same design codes	0.5	0.2	2
Same materials; Different design codes	0.35	0.14	2
Different materials; Same design codes	0.35	0.14	2
Different materials; Different design codes	0.245	0.098	2

Hurricane Andrew is a destructive Category 5 Atlantic hurricane that hit Florida, US, in August 1992. Its surface wind field at landfall (1992/8/24 9:05 according to HURDAT database [29]) is used as hazard input. It is assumed that the community center is 12.4-km west of the storm center at landfall and the y direction of the community shown in Fig. 8 is parallel to the nearby coastline of South Florida. To determine surface gust wind speeds at buildings, the surface sustained wind speeds are computed using the gradient wind field model and the gradient-surface conversion factor in Georgiou [30], and the gust factor model in Vickery and Skerlj [31] is used to convert sustained wind speeds to gust wind speeds. To apply the wind field model, hurricane key parameters are required as model input. Translation speed and direction, the location of storm center, central pressure and maximum surface wind speed, are collected or derived from HURDAT [29]. The radius to maximum wind is collected from Landsea et al. [32]. Holland parameter in the wind field model was determined such that the computed maximum surface wind speed matches the recorded value [33]. To consider the uncertainty of wind speeds, the computed wind speeds are multiplied by a lognormal random variable with a mean of 1 and a COV of 0.1 [34]. It is assumed that the bias terms at different sites are statistically independent.

4.2. The comparison between IOLE and RS

The statistics of building portfolio cost ratio Z are evaluated using three methods, i.e., the accurate method, the random sampling (RS) method [4], and the improved OLE (IOLE) method. This example has more than 20,000 buildings. It is computationally difficult to accurately simulate the correlated damages of all the buildings by constructing the correlation coefficient matrix of all the buildings. Herein, 80% of buildings are uniformly sampled from each building type in each building zone. All the sampled buildings are considered in analyzing the building portfolio loss and the estimated loss is treated as "accurate". In each building zone, for any building type, the RS method samples η percent, and the IOLE samples η percent and interpolates additional c percent. η is referred to as the sampling ratio, and c is the interpolation ratio.

For each method, MCS is applied to estimate the statistics of Z including mean loss $\overline{Z}$, standard deviation σ_Z, and the probable maximum loss (PML) of cost ratio. The PML is the loss value with a small exceedance probability (10^{-3} in this example unless specified otherwise), which is a common decision

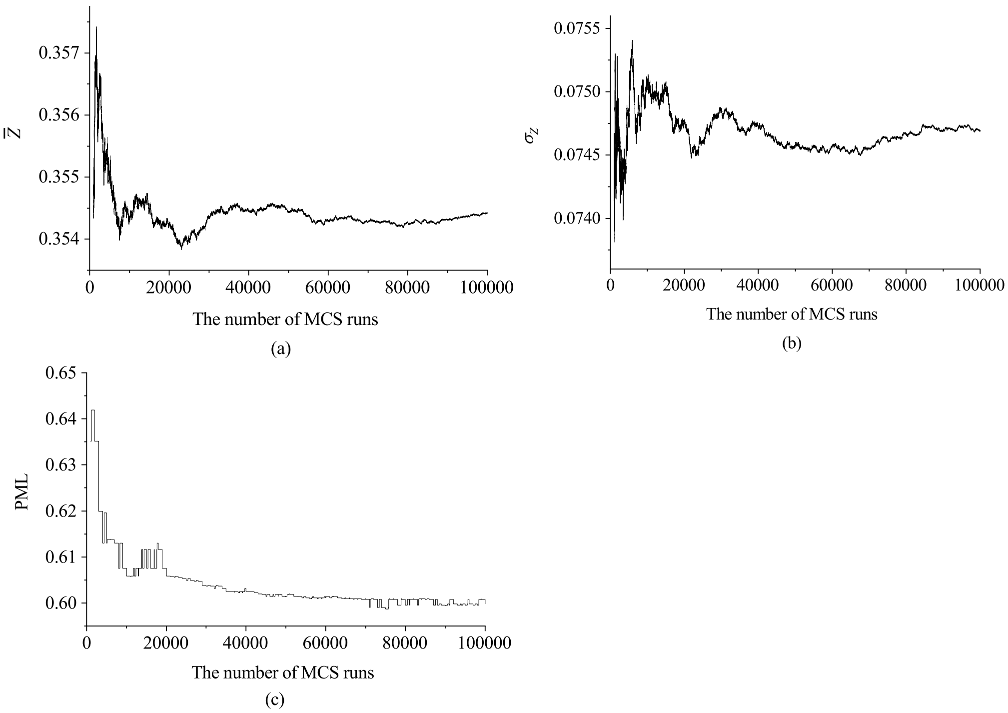

Figure 9: Example 1: The impact of MCS run in estimating (a) $\overline{Z}$, (b) σ_Z, (c) PML, for Centerville building portfolios.

metric for decision-making when financial consequences are severe [35]. To determine the suitable number of MCS runs, different numbers of MCS runs were checked when the “accurate” method was applied. Estimated statistics are given in Fig. 9. It was found that the variation of estimated statistics is negligible if more than 50,000 MCS runs are used. For example, as the number of MCS run increases from 50,000 to 100,000, the variation of the $\overline{Z}$ estimate is about 0.089%. Thus, 50,000 MCS runs were used in all the computation of this example.

IOLE and RS are first compared in estimating $\overline{Z}$, σ_Z, and PML (for an

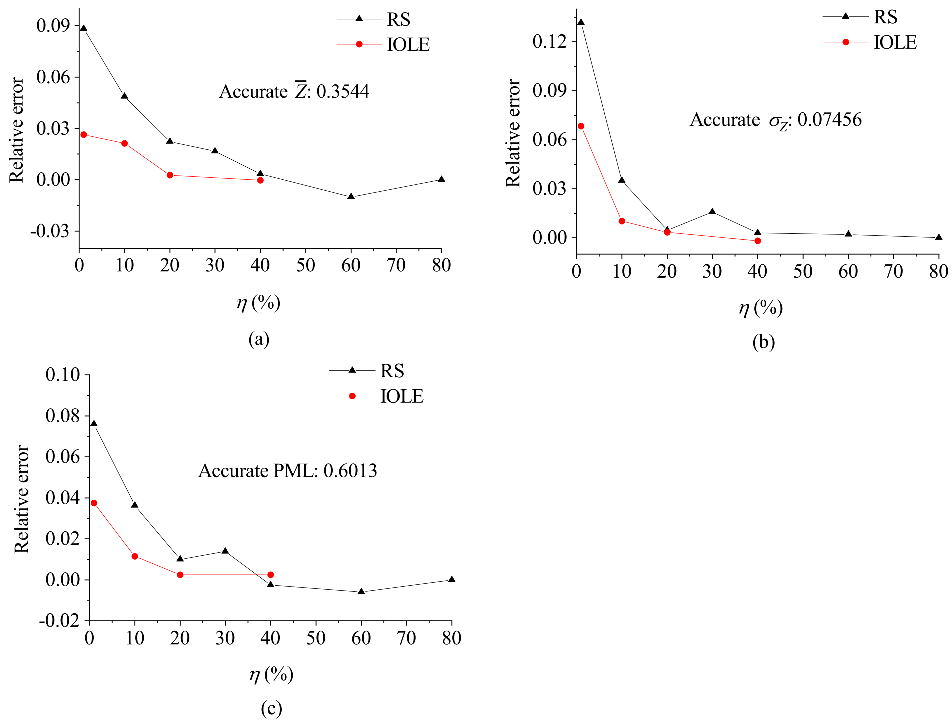

Figure 10: Example 1: comparison of RS and IOLE given different sampling ratio η, in estimating (a) $\overline{Z}$, (b) σ_Z, (c) PML, for Centerville building portfolios.

exceedance probability of 10^{-3}), given different sampling ratio η. For IOLE, the interpolation ratio c is set equal to η. Relevant results are given in Fig. 10. The advantage of the IOLE over the RS is most obvious when the number of samples are limited (i.e., $\eta < 10\%$). IOLE can generally achieve the same accuracy of RS by sampling 50% less buildings.

For further sensitivity analysis, the η of RS is set as 10%, and the η and c of IOLE are both set as 10% unless specified otherwise. First, RS and IOLE are compared in estimating the PML of different exceedance probabilities. Fig. 11 gives the complementary cumulative distribution function (CCDF)

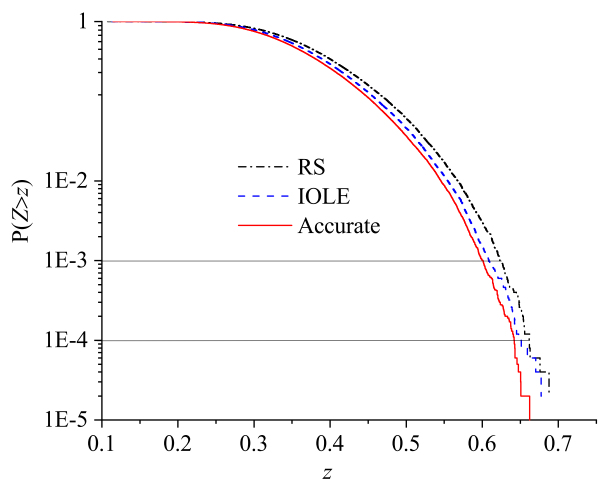

Figure 11: Example 1: CCDF of Z estimated by different methods, for Centerville building portfolios.

405 of Z solved by various methods. It is found that PML solved by IOLE is consistently more accurate than that solved by RS. Then different correlation lengths are considered. The loss statistics estimated by different methods are given in Fig. 12. It was found that the curves of IOLE, RS and the accurate method are roughly parallel to each other. The improved accuracy of IOLE, compared with RS, is not influenced by the change of correlation length. Finally, the impact of interpolation ratio c in the accuracy of IOLE is examined, with relevant results shown in Fig. 13. Again, the relative error of IOLE is always lower than that of RS. The relative error of IOLE can be further reduced by increasing c.

The above analyses adopt a simplified deterministic cost ratio for each building damage state. In practice, uncertainties exist in damage/loss values.

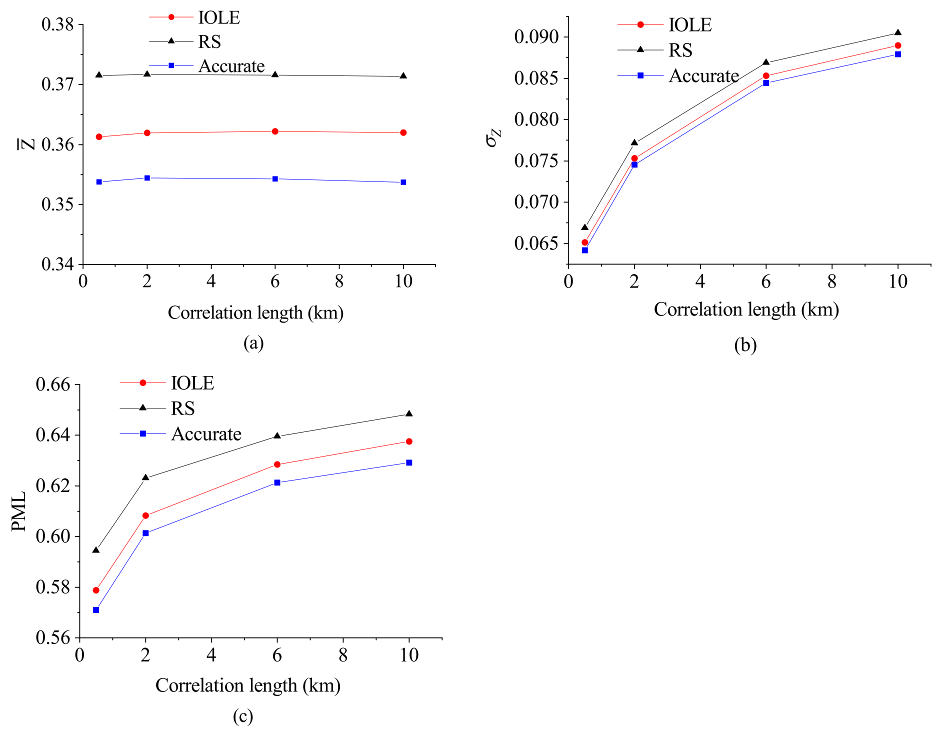

Figure 12: Example 1: comparison of RS and IOLE given different correlation length, in estimating (a) $\overline{Z}$, (b) σ_Z, (c) PML, for Centerville building portfolios.

To examine the impact of loss value uncertainty, it is assumed that the cost ratio R is a lognomal, with a mean value of 0.2 for the damage state $D = 1$, a mean of 0.4 for the damage state $D = 2$, and a mean of 0.8 for the damage state $D = 3$. The COV of the cost ratio R is assumed to be the same for each damage state, varying between 0.05 to 0.3. It was found that the COV of the cost ratio R does not affect the mean value of the building portfolio loss, and has an insignificant effect on the standard deviation of the building portfolio loss as shown in Figure 14. Figure 14 also shows that the proposed method is more accurate than the random sampling method.

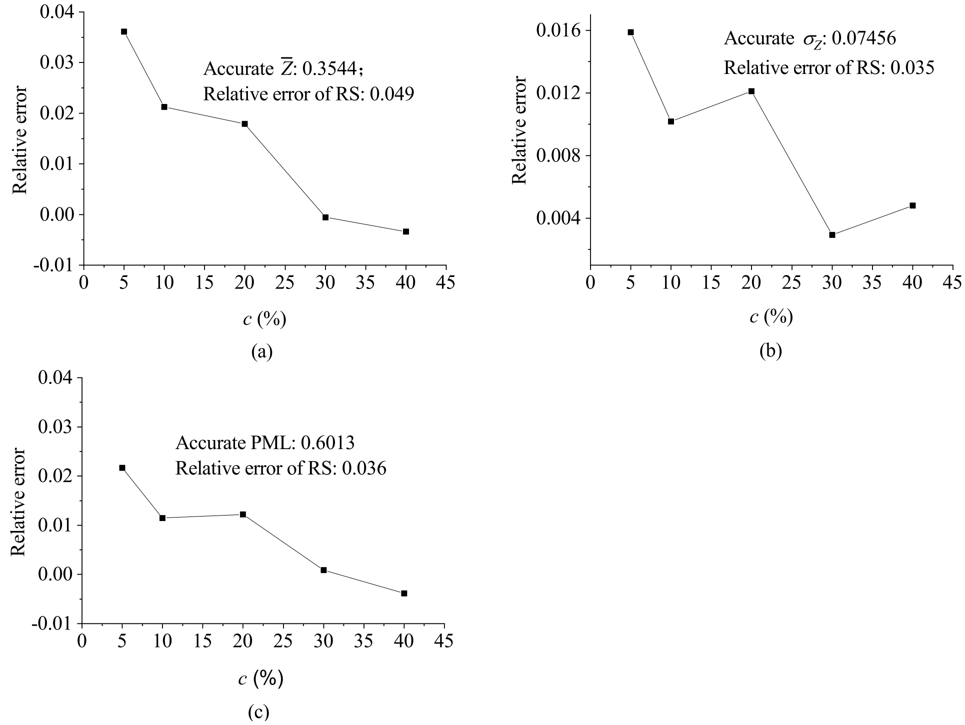

Figure 13: Example 1: accuracy of IOLE given different interpolation ratio c, in estimating (a) $\overline{Z}$, (b) σ_Z, (c) PML, for Centerville building portfolios.

In general, to simulate the correlated damages of N structures in an infrastructure system, the main computational demand is the orthogonal decomposition of the system's correlation matrix (which is $N \times N$). In the IOLE method with M focused samples, the size of the correlation matrix is reduced to $M \times M$. Consider the current example in which the building portfolio has a total of 20609 buildings. The building portfolio loss is estimated using two methods: the RS method with 40% sampling ratio, and the IOLE method with 10% sampling ratio and 30% interpolation ratio. The relative errors of both methods are below 1%. However, RS requires 1285 seconds to

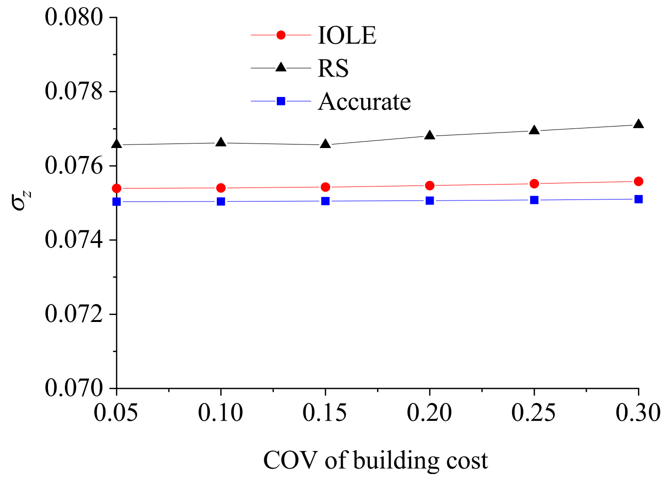

Figure 14: Example 1: comparison of RS and IOLE given different COV of cost ratio in estimating σ_Z for Centerville building portfolios.

estimate the loss, while IOLE requires 509 seconds.

It should be noted that in the RS method, only the damage/performance of the sampled components are known. Thus, RS cannot be used for connectivity analysis of lifeline networks while IOLE can, e.g. the power outage ratio of an electric power network as will be demonstrated in the next section. It is because the connectivity analysis of an infrastructure system requires the information of all the infrastructure components to capture the interdependent effects.

For practical applications, a suitable sampling ratio should be decided in order to evaluate the loss of realistic building portfolios. In the seismic loss analysis of community building portfolios in the studies of Vitoontus [36], and Vitoontus and Ellingwood [4], a smaller representative region is first modelled using different sampling ratios. For this smaller region, the required sampling ratio can be determined by comparing the approximate loss estimates with the accurate result. This sampling ratio is then used for estimating the loss of the entire community. This idea of choosing a suitable sampling ratio can be followed for application purposes.

5. Example 2: connectivity analysis of an electric power system under a scenario cyclone

The second example evaluates the performance of an electric power system under a scenario cyclone event, in which the connectivity between different infrastructure components need to be captured.

5.1. Description of the electric power system

The electric power system is based on the example of Salman and Li [37]. The topology of the power transmission grid is for the power grid in Shelby County, Tennessee, USA. In this paper, it is assumed located in a coastal region of South Carolina to consider cyclone hazard. It covers an area of about 50×42 km^2. The topological structure of the power system is shown in Fig. 15. It has 8 high-voltage gate stations, 17 medium-voltage substations, 16 low-voltage substations and 12 intersections of transmission lines, along with 66 transmission lines. Since there is no energy generating plant in this system, the gate stations are assumed as supply nodes that provide electricity for substations. It should be noted that the gate nodes are typically boundary points to a larger power transmission grid whose energy generation plants are located elsewhere.

The medium-voltage and low-voltage substations are demand nodes that directly serve the customers in their neighbourhoods. The span of a transmis-

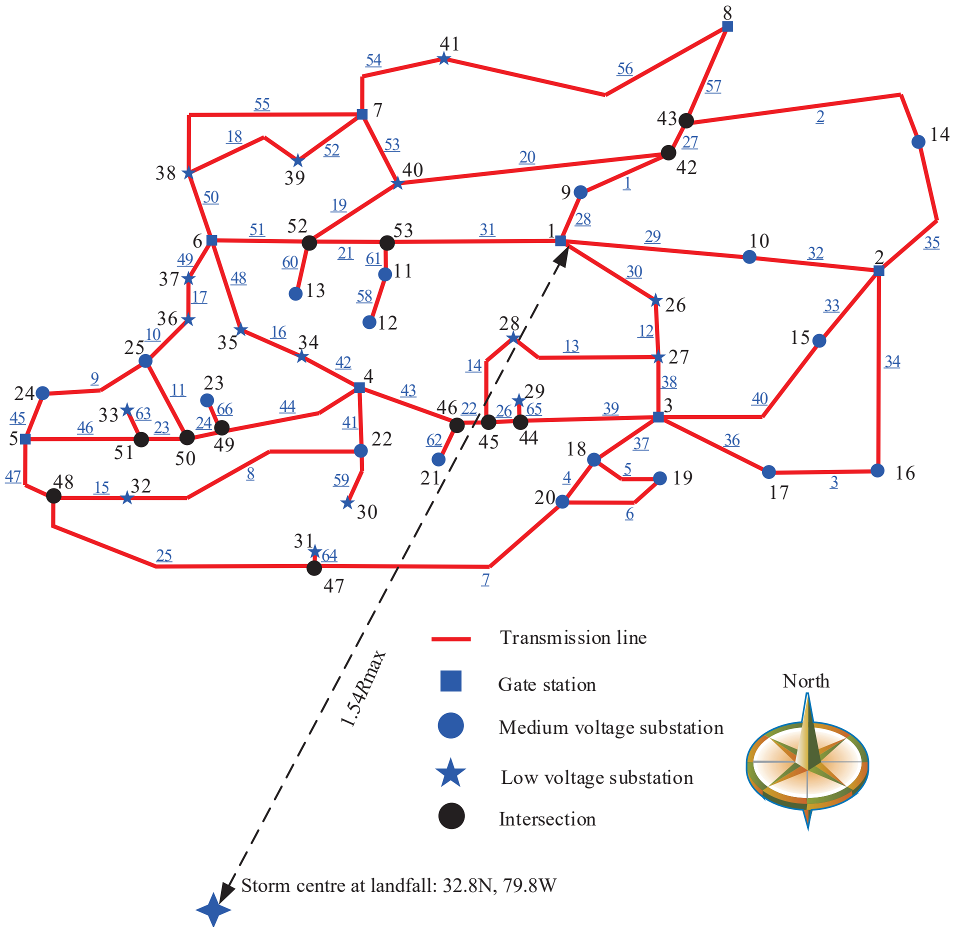

Figure 15: Example 2: an electric power system (modified from Salman and Li [37]) and the storm centre location of Hurricane Hugo (1989) ($R_{\max}$: radius to maximum wind).

sion line between two transmission support structures is assumed to be 244 m. There are 1767 transmission line-supporting structures in total. Wind-induced damage to the support structures is considered, since they are the most vulnerable structures under wind effects. The fragility function of the transmission support structures is taken from Brown [38] as follows,

$$P(D = 1|U = u) = \min\left(2 \cdot 10^{-7}\exp(0.1866u), 1\right), \tag{15}$$

in which D is the binary damage state of a transmission support structure, equal to 0 for no damage and 1 for failure, and U is the 3-s gust wind speed in m/s. The fragility functions for any two transmission support structures i and j are modelled as correlated, with a correlation function of Eq. (14), in which $a = 0.5$, $r = 0.2$, and the correlation length $b = 15$ km. It should be noted that the parameter values of correlation model are chosen for demonstration purpose. Sensitivity analysis will be conducted in the next section.

Hurricane Hugo was chosen as the scenario event. The hurricane made landfall in South Carolina as a Category 4 storm at 4:00 AM on September 22, 1989. The location of the storm centre at landfall relative to the electric power system is shown in Fig. 15. Note that gate station 1 is located 20 km to the east of the storm centre and 60 km to the north of the storm centre. The maximum surface gust wind speed of each transmission support structure during the hurricane passage was used to determine structural damage. To this end,the time history of surface wind speed at each structure was first sought in an interval of 30 minutes using the wind models same as those of the building portfolio example, and then the maximum wind speed was found. The key hurricane parameters, including storm translation direction and speed, the latitude of storm center, central pressure and maximum surface wind speed, were collected or derived from HURDAT database [29]. Since HURDAT only provides the records of hurricane key parameters in an interval of 6 hours, the records in a 30-minute interval are obtained by linear interpolation [37]. The radius to maximum wind is estimated using the empirical formula from Vickery and Wadhera [33]. The Holland parameter in the wind field model was determined such that the computed maximum surface wind speed matches the recorded value [33]. This study considered the path of the hurricane from 0:00 to 12:00 on September 22, 1989 and found that considering this path segment is enough to capture the maximum wind speed of each structure during the storm passage. To consider wind speed uncertainty, the lognormal distribution, same as that of the building portfolio example, was used.

The performance of the power system is measured using the power outage ratio, Q, the ratio of the customers losing access to power to the total customers, as follows

$$Q = \frac{\sum_{j=1}^{N'} r_j F_j}{\sum_{j=1}^{N'} r_j}, \tag{16}$$

in which r_j is the number of the customers served by demand node j, F_j indicates the functional state of demand node j, 1 for failure and 0 for functional, and N' is the total number of demand nodes. It is assumed that a demand node fails if it loses connection to all supply nodes, and functions if it is connected to at least one supply node. One low-voltage substation serves 10,000 customers and one medium-voltage substation serves 14,000 customers. In total, there are 398,000 customers served by the power system. Transmission lines connecting to a supply node are unidirectional and electricity can only transmit from the supply nodes to the demand nodes. Transmission lines connected to terminal substations such as nodes 12 and 13 in Fig. 15 are also unidirectional and electricity is transmitted to terminal substations. Other transmission lines are bi-directional. A transmission line connecting two nodes is modelled as a series system with multiple transmission support structures. If any of the transmission support structures is damaged, all transmission lines supported by the structure fail. The failed lines are removed from the network and the status of the demand node F_j is determined using a shortest path algorithm which searches for the available path(s) from any supply node to the demand node.

5.2. The performance of IOLE

The performance of the IOLE method was examined in estimating the power outage ratio Q of the system. To apply the IOLE method, η percent of transmission support structures are sampled and their damage is obtained accurately. Damages to the remaining $(100 - \eta)$ percent of the support structures are interpolated. In the current example, the η percent of structures include two parts. The first part contains all the support structures located at the intersections of transmission lines (marked as black solid circle in Fig. 15), accounting for 0.68% of all the support structures. The other $(\eta - 0.68)$ percent of structures are uniformly sampled along each transmission line. To demonstrate the accuracy of IOLE, the accurate method is also used in which the full correlation coefficient matrix of all the support structures is constructed and used to simulate the correlated damages to the support structures. MCS is used to estimate the statistics of Q. Different runs of MCS were checked, when the accurate method was applied. It is found that 10^5 MCS runs are sufficient to stably estimate the mean $\overline{Q}$ and the standard deviation σ_Q of Q. In all the computation of this example, 10^5 MCS were used.

The IOLE was used to estimate the statistics of Q given different sampling ratio η, in comparision with the accurate method. Results are shown in

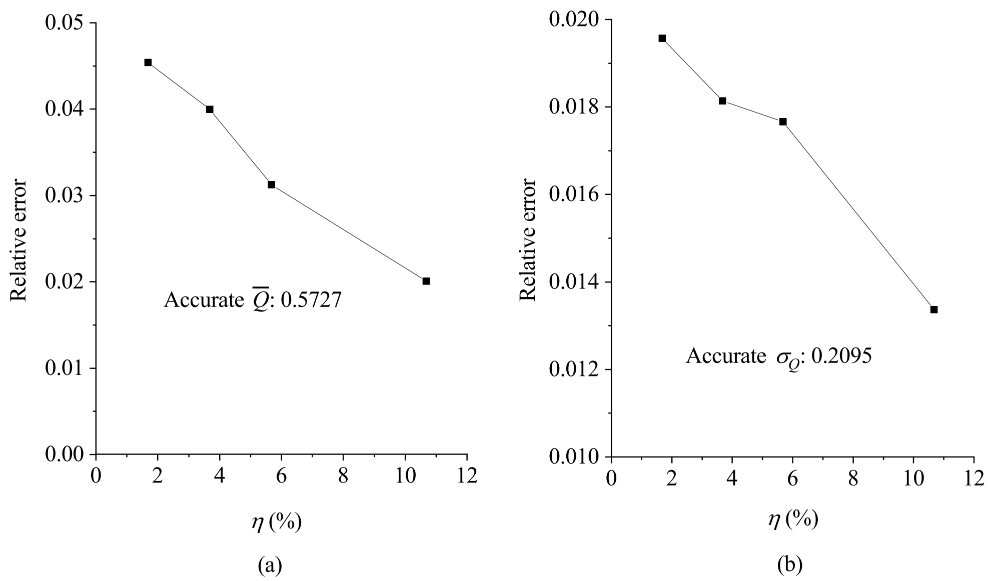

Figure 16: Example 2: relative errors of IOLE using different sampling ratio η, (a) $\overline{Q}$, (b) σ_Q.

Fig. 16. From the accurate method, the power outage ratio Q has a mean of 0.57 with a standard deviation of 0.21, suggesting that on average 57% of the customers would lose access to power. The accuracy of IOLE improves as η increases. The relative errors in $\overline{Q}$ and σ_Q are below 5% when η is just 2%. If the sampling ratio is further increased to 11%, the errors can be controlled below 2%. The results demonstrate that the IOLE can be used for utility networks with interconnected infrastructure components.

The accuracy of IOLE was further examined by considering different correlation lengths. Fig. 17 compares the accurate method, and the IOLE

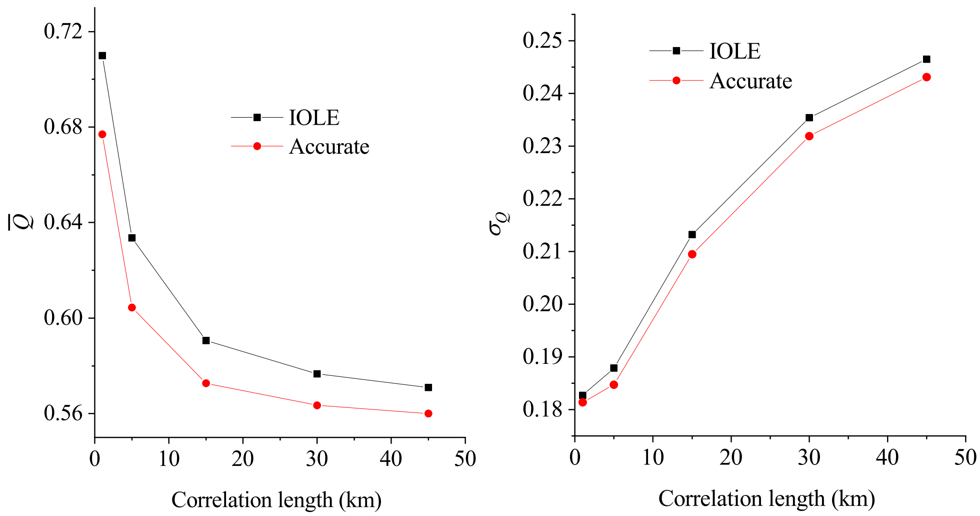

(a) (b)

Figure 17: Example 2: Comparison between the IOLE and accurate methods given different correlation lengths, (a) $\overline{Q}$, (b) σ_Q.

method by sampling 5% structures in addition to the structures at the intersections of tranmission lines. The discrepancy between the two methods roughly remains constant with an increasing correlation length, indicating that the accuracy of IOLE is insensitive to the change of correlation length.

6. Conclusion

The improved optimal linear estimation method can simulate non-differentiable random fields. The technique can be used for risk assessment of large-scale infrastructure systems with correlated components, as demonstrated by two examples.

Example 1 evaluates the cyclone repair costs of building portfolios in the virtual community Centerville. It was found that the accuracy of both the IOLE and the RS methods increases as the sampling ratio increases. However, for very small sampling ratios (i.e., $\eta \leq 10\%$), the accuracy of the RS is rather poor, while the IOLE can still give reasonable results. Also, sensitivity analysis on the threshold value of PML, correlation length and the interpolation ratio of IOLE has been conducted. The accuracy of IOLE was found consistently higher than that of RS.

The most significant advantage of the IOLE over the conventional random sampling method is that it can handle the connectivity analysis of complex systems. This point is demonstrated using the electric power distribution system in Example 2. The conventional random sampling method cannot be used for this example, as assessing the system requires the information of all components in the system. For the IOLE, the relative errors of the mean and standard deviation of the power outage ratio can be controled below 5% by using a sampling ratio of just 2% . The accuracy of IOLE remains given different values of correlation length.

Acknowledgements

This research has been supported by the Faculty of Engineering and IT PhD Research Scholarship from the University of Sydney. This support is gratefully acknowledged.

References

[1] T. McAllister, Developing guidelines and standards for disaster resilience of the built environment: A research needs assessment, US Department of Commerce, National Institute of Standards and Technology, 2013.

[2] K. H. Lee, D. V. Rosowsky, Fragility assessment for roof sheathing failure in high wind regions, Eng Struct 27 (6) (2005) 857–868.

[3] Y. Li, B. R. Ellingwood, Hurricane damage to residential construction in the US: Importance of uncertainty modeling in risk assessment, Eng Struct 28 (7) (2006) 1009–1018.

[4] S. Vitoontus, B. R. Ellingwood, Role of correlation in seismic demand and building damage in estimating losses under scenario earthquakes, in: Proceedings of 11th International Conference on Structural Safety & Reliability (ICOSSAR 2013), New York, NY: AA Balkema, 2013.

[5] K. Goda, H. Hong, Estimation of seismic loss for spatially distributed buildings, Earthquake Spectra 24 (4) (2008) 889–910.

[6] H. Bonstrom, R. B. Corotis, Building portfolio seismic loss assessment using the first-order reliability method, Struct Saf 52 (2015) 113–120.

[7] G. A. Weatherill, V. Silva, H. Crowley, P. Bazzurro, Exploring the impact of spatial correlations and uncertainties for portfolio analysis in probabilistic seismic loss estimation, Bulletin of Earthquake Engineering 13 (2015) 957–981.

[8] C. Kang, O. Kwon, J. Song, Evaluation of correlation between engineering demand parameters of structures for seismic system reliability analysis, Struct Saf 93 (2021) 102133.

[9] T. Adachi, B. R. Ellingwood, Serviceability assessment of a municipal water system under spatially correlated seismic intensities, Computer-Aided Civil and Infrastructure Engineering 24 (2009) 237–248.

[10] N. Jayaram, J. W. Baker, Efficient sampling and data reduction techniques for probabilistic seismic lifeline risk assessment, Earthquake Eng Struct Dyn 39 (2010) 1109–1131.

[11] C. Wang, K. Feng, H. Zhang, Q. Li, Seismic performance assessment of electric power systems subjected to spatially correlated earthquake excitations, Structure and Infrastructure Engineering 15 (2019) 351–361.

[12] D. Zeng, H. Zhang, Q. Li, B. R. Ellingwood, Tropical cyclone damage assessment of distributed infrastructure systems under spatially correlated wind speeds, Struct Saf 91 102080.

[13] R. Lee, A. S. Kiremidjian, Uncertainty and correlation for loss assessment of spatially distributed systems, Earthquake Spectra 23 (4) (2007) 753–770.

[14] J. Ghosh, K. Rokneddin, J. E. Padgett, L. Dueñas-Osorio, Seismic reliability assessment of aging highway bridge networks with field instrumentation data and correlated failures, I: Methodology, Earthquake Spectra 30 (2) (2014) 795–817.

[15] P. Lin, N. Wang, B. R. Ellingwood, A risk de-aggregation framework that relates community resilience goals to building performance objectives, Sustainable and Resilient Infrastructure 1 (1-2) (2016) 1–13.

[16] C. Wang, H. Zhang, B. R. Ellingwood, Y. Guo, H. Mahmoud, Q. Li, Assessing post-hazard damage costs to a community's residential buildings exposed to tropical cyclones, Structure and Infrastructure Engineering 17 (2021) 443–453.

[17] T. Adachi, Impact of cascading failures on performance assessment of civil infrastructure systems, Ph.D. thesis, Georgia Institute of Technology (2007).

[18] K. Rokneddin, J. Ghosh, L. Dueñas-Osorio, J. E. Padgett, Seismic reliability assessment of aging highway bridge networks with field instrumentation data and correlated failures, II: Application, Earthquake Spectra 30 (2) (2014) 819–843.

[19] D. Zeng, H. Zhang, C. Wang, Modelling correlated damage of spatially distributed building portfolios under scenario tropical cyclones, Struct Saf 87 (2020) 101978.

[20] P. Lin, N. Wang, Building portfolio fragility functions to support scalable community resilience assessment, Sustainable and Resilient Infrastructure 1 (3-4) (2016) 108–122.

[21] C. C. Li, A. Der Kiureghian, Optimal discretization of random fields, J Engrg Mech 119 (6) (1993) 1136–1154.

[22] C. Wang, H. Zhang, Roles of load temporal correlation and deterioration-load dependency in structural time-dependent reliability, Comput Struct 194 (2018) 48–59.

[23] F. Wang, H. Li, System reliability under prescribed marginals and correlations: Are we correct about the effect of correlations?, Reliability Engineering and System Safety 173 (2018) 94–104.

[24] N. J. Higham, Computing the nearest correlation matrix—a problem from finance, IMA Journal of Numerical Analysis 22 (2002) 329–343.

[25] R. E. Melchers, A. T. Beck, Structural reliability analysis and prediction, John Wiley & Sons, 2018.

[26] B. R. Ellingwood, H. Cutler, P. Gardoni, W. Peacock, J. W. van de Lindt, N. Wang, The Centerville Virtual Community: a fully integrated decision model of interacting physical and social infrastructure systems, Sustainable and Resilient Infrastructure 1 (3-4) (2016) 95–107.

[27] C. Wang, Time-dependent reliability of aging structures: From individual facilities to a community, Ph.D. thesis, The University of Sydney (2019).

[28] FEMA, Multi-hazard loss estimation methodology, hurricane model (HAZUS-MH 2.1), Technical manual, Federal Emergency Management Agency, Washington, D. C., 2014.

[29] HRD/NOAA, Detailed list of continental United States hurricane impacts/landfalls 1851-1960, 1983-2020, http://www.aoml.noaa.gov/hrd/hurdat/hurdat2.html[Accessed: 15 September, 2021] (2020).

[30] P. N. Georgiou, Design wind speeds in tropical cyclone-prone regions, Ph.D. thesis, University of Western Ontario (1986).

[31] P. J. Vickery, P. F. Skerlj, Hurricane gust factors revisited, J Struct Eng 131 (5) (2005) 825–832.

[32] C. W. Landsea, J. L. Franklin, C. J. McAdie, J. L. Beven, J. M. Gross, B. R. Jarvinen, R. J. Pasch, E. N. Rappaport, J. P. Dunion, P. P. Dodge, A reanalysis of Hurricane Andrew's intensity, Bulletin of the American Meteorological Society 85 (11) (2004) 1699–1712.

[33] P. J. Vickery, D. Wadhera, Statistical models of Holland pressure profile parameter and radius to maximum winds of hurricanes from flight-level pressure and H*Wind data, Journal of Applied Meteorology and Climatology 47 (10) (2008) 2497–2517.

[34] P. J. Vickery, D. Wadhera, L. A. Twisdale Jr, F. M. Lavelle, US hurricane wind speed risk and uncertainty, J Struct Eng 135 (3) (2009) 301–320.

[35] P. Grossi, H. Kunreuther, Catastrophe modeling: a new approach to managing risk, Springer, New York, 2005.

[36] S. Vitoontus, Risk assessment of building inventories exposed to large scale natural hazards, Ph.D. thesis, Georgia Institute of Technology (2012).

[37] A. M. Salman, Y. Li, Multihazard risk assessment of electric power systems, J Struct Eng 143 (3) (2016) 04016198.

[38] R. E. Brown, Cost-benefit analysis of the deployment of utility infrastructure upgrades and storm hardening programs, Tech. rep., Quanta Technology, Raleigh (2009).